Design and analysis of beam steering multicore fiber optical switches

Callum Deakin, Michael Enrico, Nick Parsons, Georgios Zervas

***Abstract*—The design and performance characteristics of a beam steering optical switch for multicore fibers (MCFs) are reported. Port count, core count, transmission crosstalk or a combination thereof can be optimized for the required application. Decreasing port separation or increasing the maximum steering angle both increase port count, whilst a higher core count or larger mode field diameter increase port capacity or port count respectively at the expense of greater intercore crosstalk. Potential losses from system misalignments and fiber fabrication variations in the core pitch are also estimated. A 50 port switch is possible for a $25\,\mu\mathrm{m}$ core pitch 7 core hexagonal trench assisted MCF (TA-MCF) with a total mean statistical crosstalk on the central core of -25 dB after 1 km, assuming a operational wavelength of 1550 nm and maximum collimator actuator angle of 10 degrees. In contrast, a high capacity $25\,\mu\mathrm{m}$ core pitch 61 core hexagonal TA-MCF can still offer up to a 5 port switch for the same level of crosstalk. For longer link distances, -25 dB crosstalk after 100 km (metro network) is achievable for a 50 port switch using a $35\,\mu\mathrm{m}$ core pitch 7 core TA-MCF. Similar levels of crosstalk can be accomplished at 1000 km (core network) for a 41 port switch using a $35\,\mu\mathrm{m}$ core pitch 7 core TA-MCF.**

***Index Terms*—Multicore fiber, Optical fiber switches, Beam steering.**

I. Introduction

THE persistent growth of internet protocol traffic means that traditional single mode fibers (SMF) are reaching their fundamental capacity limit [1]. This problem is particularly acute in data center networks (DCNs), where the spatial efficiency, cost and power consumption requirements of SMFs are especially restrictive.

One promising technology to expand fiber capacity and sustain this growth is spatial division multiplexing (SDM) [2]. Uncoupled multicore fibers (MCFs) are one of the simplest ways to achieve SDM within single fiber and as such have been the focus of many research efforts within the last decade. Many investigations have focused on optimizing the design of MCFs for multicore transmission: specifically to maximize core density whilst minimizing intercore crosstalk [3], through the use of trench assisted (TA) cores [4], [5], heterogeneous fiber designs [6] and hole assisted structures [7]. The use of MCFs in DCNs could reduce cost and power consumption of transceiver digital signal processing and offer increased front panel density [8], [9], [10].

Manuscript submitted September 25, 2018. This work was supported by the EPSRC project TRANSNET (EP/R035342/1).

C. Deakin (e-mail: callum.deakin.17@ucl.ac.uk) and G. Zervas (email: g.zervas@ucl.ac.uk) are with the Department of Electronic and Electrical Engineering, University College London, London WC1E 7JE, UK.

M. Enrico and N. Parsons are with Polatis Ltd, Cambridge, CB4 0WN, UK.

The deployment of MCFs as spatial superchannels to meet traffic demands in core networks or DCNs would require highly scalable photonic cross connects [11]. Yet switches for these MCF systems often rely on single mode switching technologies with additional stages for SDM multiplexing/demultiplexing [12], [13], [14], [15]. Recently however, a free space beam steering optical switch that directly integrates MCFs and avoids the need for SDM multiplexing components has been demonstrated. Removing the multiplexing/demultiplexing stages would significantly reduce the switch complexity and losses from fan in/out devices, as well as increasing the bandwidth density of the switch. Such a high bandwidth density switch could be utilized for connections between high capacity DCN devices such as serial memory elements [16], as well the switching of spatial superchannels in core and metro networks [11]. On the other hand, integrating high core count MCFs into the switch also faces significant practical challenges such as increased sensitivity to switch misalignment and losses caused by variation in the core pitch, which are explored in this paper.

The switch configuration was first described in [17] and is shown in Fig. 1. The basic layout consists of a folded telecentric lens configuration created by a mirror and micro lens array, consisting of lenses of focal length $f_2/2$ giving effective focal length f_2 due to the double pass configuration. These lenses are spaced at half the collimator pitch to ensure that any beam traveling between ports passes through the center of a lens in the array. Note that the switch can also be arranged in an unfolded configuration: i.e. without a mirror and with two sets of a collimator arrays.

The MCFs are coupled into lens collimators with focal length f_1 and steered using individual piezo actuators via a low stress flexure pivot. This configuration allows for low loss non blocking connectivity between MCFs arranged in a 2D array, with 384 ports being realized for SMFs. Ports are connected by applying voltages to the two independent actuators controlling the angle of the collimators in the x and y directions to align the input and output collimators. Connectivity is independent of the direction or power of the light and reconfiguration time is of the order of milliseconds [18].

To achieve a telecentric configuration and ensure optimal coupling between the two MCFs, the distance from the fiber output to collimating lens must be set to $z_1 = f_1(1 + f_1/f_2)$ and the distance from the collimating lens to the lens array must be set to $z_2 = f_1 + 2f_2$. This ensures that the lens array performs a 1:1 imaging from one fiber end face to another.

When designing the switch, there are three main performance parameters that need to be considered:

This article has been accepted for publication in a future issue of this journal, but has not been fully edited. Content may change prior to final publication. Citation information: DOI 10.1109/JLT.2019.2896318, Journal of Lightwave Technology

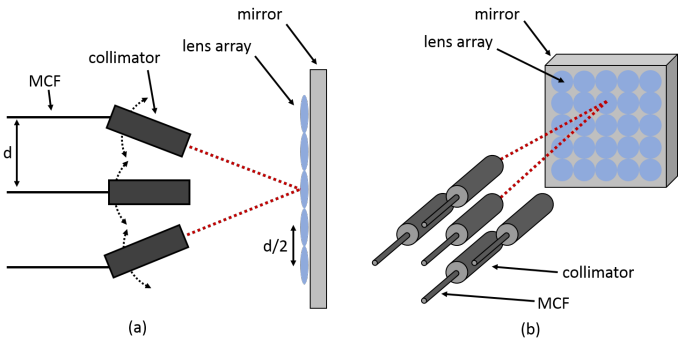

Fig. 1. (a) A one dimensional slice of the switch configuration with the overall structure shown in (b). Fiber collimators are steered by piezo actuators to pass through the center of the lenses within the array and imaged onto the exit fiber end face. Example beam paths are shown in red.

1) Intercore **crosstalk**, determined by the coupling between cores within the fiber.
2) Maximum **connectivity** of the switch, represented by the number of input to output ports, or port count.
3) Maximum **capacity** of each port, represented by the number of cores which in turn determines the potential throughput of each port.

These three parameters are necessarily in conflict and the importance of each is determined by the specific application. For example, intra-data center applications require high throughput and connectivity at the expense of increased crosstalk, whilst long haul communications cannot tolerate high crosstalk fiber designs and must sacrifice fiber capacity or connectivity. This is in addition to the loss induced by the switch which, depending on the loss mechanism, may or may not depend on how these parameters have been configured.

In this paper we explore how each of these parameters can be optimized in the design of the switch and what penalty this imposes on the others. We examine a 1 dimensional slice, i.e. a single row or column of the collimator array in Fig. 1(b), with the assumption this can be expanded to a 2 dimensional array using the same specifications in the new dimension. Thus a reference to port count of N in the following sections can be assumed to be scalable to a 2D array of equal spacing in both Cartesian directions, with the total number of ports given by

$$N_{(2)} = \text{ceil}\left[\frac{N^2}{2}\right] \tag{1}$$

where ceil denotes the ceiling function. This relationship derives from the fact that the size of the array is limited by the connection between the two most extreme ports, and is illustrated by Fig. 2. This 2D array of $N_{(2)}$ collimators could be deployed in the folded or unfolded configuration to form a $N_{(2)}$ port switch or $N_{(2)} \times N_{(2)}$ port switch respectively. The folded configuration utilizes a single array to allow a connection between any of the $N_{(2)}$ ports, whilst an unfolded configuration allows $N_{(2)}$ input ports to be cross connected to $N_{(2)}$ output ports. Throughout this paper, a reference to a $N_{(2)}$ port count switch can therefore be assumed to be employable in either configuration. This 2D port count is the maximum

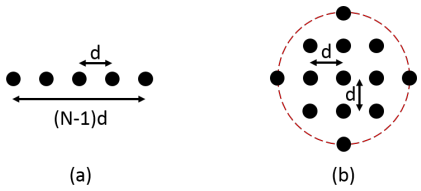

Fig. 2. A (a) 1D slice of N collimators spaced at d can be scaled to a (b) 2D array of $N_{(2)}$ collimators spaced at d.

possible and may be reduced in a practical implementation due to manufacturing or packaging constraints.

In Section 2 a ray tracing model is used to explore how the geometry of the switch affects its maximum connectivity and the impact of potential loss mechanisms, whilst Section 3 describes how the fiber design influences all three of these parameters.

II. Switch Geometry

The switch was modeled as a simple system of three thin lenses, with the beam propagation calculated using ray transfer matrix analysis, assuming the paraxial approximation [19], [20]. Light exiting from each core was modeled as a monochromatic Gaussian beam, which can be realized in a ray tracing model by tracking the propagation of two paraxial rays. We assume that the beams are symmetric and so only perform calculations in 2 spatial dimensions, although in principal the technique can be extended to asymmetric beams by incorporating additional rays [21]. The mode field diameter (MFD) of the mode within each core is used as the value for the beam waist.

An example system is shown in Fig. 3, for a MCF in a switch using lenses with $f_1 = 3.52$ mm and $f_2 = 35.2$ mm. The two outer cores are separated from the central core at a pitch of $35\,\mu\text{m}$ and have a MFD of $12\,\mu\text{m}$, with the lens spacing set at the ideal distances of $z_1 = 3.70$ mm and $z_2 = 73.9$ mm.

In reality however, the distance z_2 will be variable in a dynamic switch since the beam propagates at the angle required to make a connection to another port in the array, increasing the effective value of z_2 by the relation:

$$z_2' = \frac{z_2}{\cos\theta} \tag{2}$$

Where θ is the angle the collimator makes with the optical axis. This increase is at its maximum when a connection is made between the two outer most ports in the array since this is when the largest value of θ occurs. Ports in the center of the array do not require such a large angle since the maximum lateral movement required to make a connection to any other port in the array is only half the overall width of the array. This suggests that greater port density could be achieved by reducing the distance between ports in the center of the array, but a non-uniform port array would mean that it is impossible to ensure that the beam always passes through the center of a lens in the lens array for all connections.

In this study therefore we assume that the ports are always uniformly spaced. Fig. 4 shows the value of z_2 as a function

This article has been accepted for publication in a future issue of this journal, but has not been fully edited. Content may change prior to final publication. Citation information: DOI 10.1109/JLT.2019.2896318, Journal of Lightwave Technology

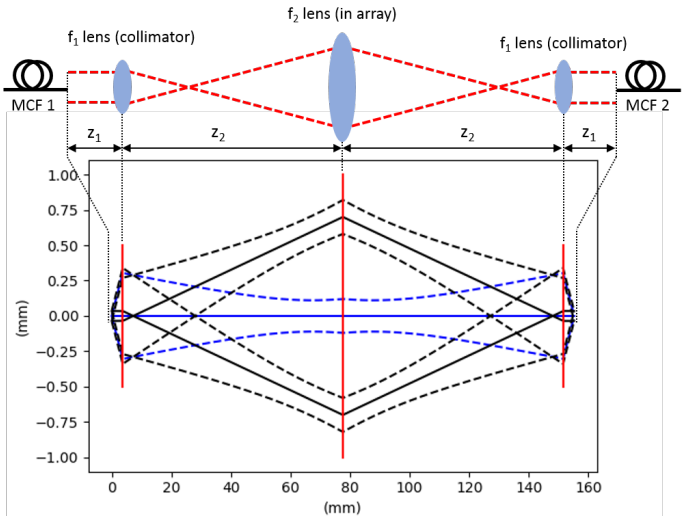

Fig. 3. Switch beam propagation model for a 12 µm MFD 7 core hexagonal homogeneous MCF with $f_1 = 3.52$ mm and $f_2 = 35.2$ mm giving $z_1 = 3.70$ mm and $z_2 = 73.9$ mm. Blue lines indicate the central core, with black lines indicating the outer core. Solid lines indicate the center of the beam whilst dashed lines indicate the $1/e^2$ intensity edge. Red vertical lines indicate the position and width of the lenses. A schematic of the lens arrangement is shown above (not to scale) for clarity.

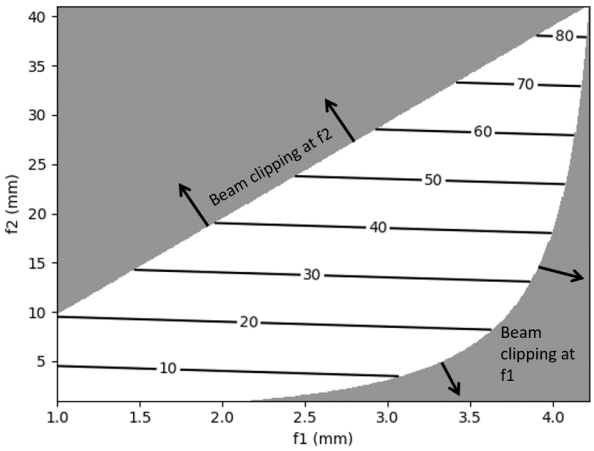

Fig. 4. z_2(mm) as a function of f_1 and f_2. The maximum value of z_2 occurs at the maximum possible values of f_1 and f_2 which are in turn restricted by the beam clipping at their respective lenses.

of f_1 and f_2 for a MCF whose outermost core is 35 µm from the center of the fiber and the MFD is 12 µm. z_2 is directly related to port count since it determines the maximum lateral movement across the port array that a beam launched at a specific angle. z_2 must therefore always be maximized in order to maximize the port count.

The maximum values of f_1 and f_2 and therefore z_2 and port count are restricted by the width of the lenses used, in this case 2 mm for lens array and 1 mm for the collimator lenses which are kept fixed throughout this paper. A large focal length for either lens means that the beams from the outer core of the MCF spread beyond the lens aperture and results in beam clipping. In this work we ensure a 5% margin

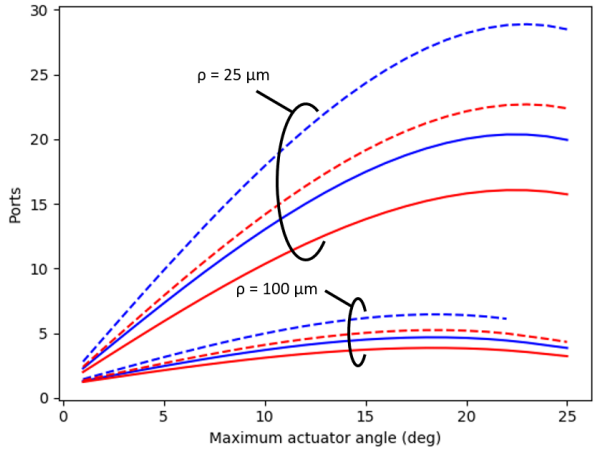

Fig. 5. Maximum number of ports in a single dimension as a function of the maximum actuator angle, with port spacing of 4mm. The f_1/f_2 values are optimized for each angle. Dashed lines indicate a MFD of 12 µm, solid lines indicate a MFD of 8 µm. Red lines are wavelength of 1620 nm, blue lines are 1260 nm. ρ is the distance from the outer most core to the fiber center.

to prevent any issues with beam distortion that could occur when passing through the edge of the lens: a larger or smaller margin will allow for less or more ports respectively.

Fig. 5 shows the dependence of the maximum port count (in 1 dimension) on the maximum angle of the collimator achievable by the actuator. Generally, increasing the maximum actuator angle leads to increase in port count due to the larger lateral movement across the array achievable by the beam. However, this reaches a maximum once the angle becomes large enough to ensure that the gains made in lateral movement are offset by beam clipping within the imaging system caused by the large increase in the effective value of z_2 and a reduction in the apparent lens aperture size.

This maximum is delayed for a larger MFD since the beam spreading is reduced. A reduction in the beam spreading means that the system can handle a larger deviation from the ideal z_2 before beam clipping occurs. This maximum is delayed to a larger degree by a decrease in the distance from the outer most core to the fiber center, represented by ρ. A more compact MCF layout allows for a large value of f_1 to be used and decrease the beam spreading between the collimator and lens array, further increasing the tolerance to deviation from the ideal z_2.

Fig. 6 shows the 1 dimensional port count dependence on the port separation. Clearly, increasing the separation above the minimum of 4 mm (dictated by the f_2 lens width of 2 mm) leads to a significant reduction in the available ports, especially for high port count systems utilizing compact MCF designs and/or short wavelengths and large MFDs. Note that the use of smaller f_2 lenses can reduce the minimum separation further but the gains in port count are negligible as this makes the system more vulnerable to beam clipping at the lens array. In practice, this minimum separation is also likely to be affected by space for piezo actuators to control the collimator angle and any necessary supporting electronics.

This article has been accepted for publication in a future issue of this journal, but has not been fully edited. Content may change prior to final publication. Citation information: DOI 10.1109/JLT.2019.2896318, Journal of Lightwave Technology

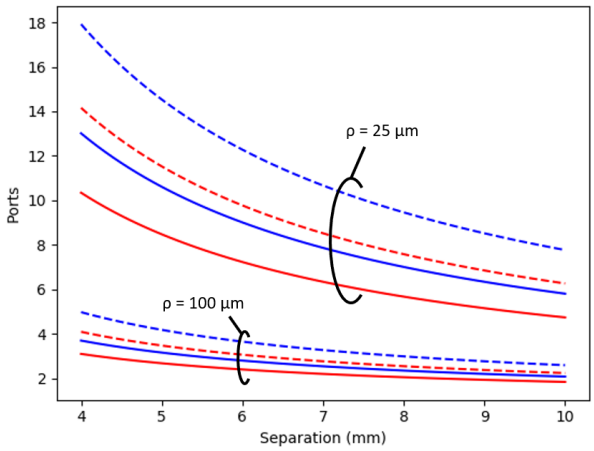

Fig. 6. Maximum number of ports in a single dimension as a function of the port separation, with maximum actuator angle set to 10 degrees. Dashed lines indicate a MFD of 12 µm, solid lines indicate a MFD of 8 µm. Red lines are wavelength of 1620 nm, blue lines are 1260 nm. ρ is the distance from the outer most core to the fiber center.

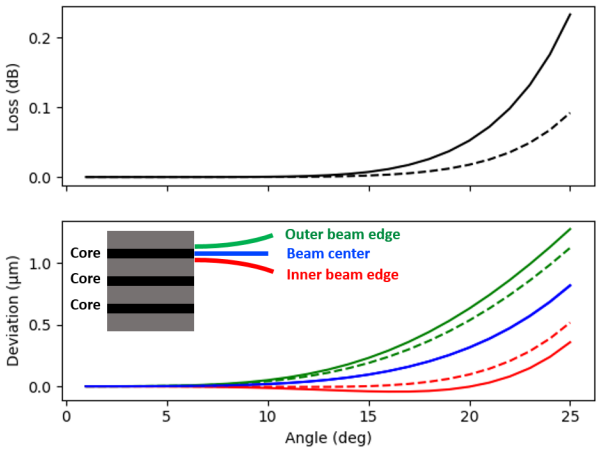

Fig. 7. Deviation of beam center and $1/e^2$ edges versus actuator angle with corresponding estimated total loss from mode field diameter mismatch and lateral displacement. Dashed lines indicate a MFD of 12 µm, solid lines indicate a MFD of 8 µm. Red lines represent the edge of the beam closest to the fiber center, green the outer edge and blue the center of the beam. The f_1/f_2 values are optimized for each angle. The deviation and loss is wavelength independent.

Aside from increasing the effective value of z_2 and leading to potential beam clipping at the lenses, deviation from the ideal imaging system displayed in Fig. 3 also causes distortion to the image created at the exit fiber end face. This is demonstrated in Fig. 7, which shows the deviation of the beam center and $1/e^2$ intensity edges from their ideal positions on the exit fiber end face, along with the corresponding estimated loss, which we approximate using the formulae

$$L_{lat} = -10 \log \left[e^{-\left(\frac{2d}{w_0}\right)^2} \right] \tag{3}$$

$$L_{mode} = -10 \log \left[\frac{4}{\left(\frac{w_0}{w_1} + \frac{w_1}{w_0}\right)^2} \right] \tag{4}$$

Where L_{lat} and L_{mode} represent the losses induced by lateral displacement and mode field diameter mismatch respectively. d is the lateral displacement of the beam from the exit fiber core, w_0 is the mode field diameter within the fiber core and w_1 is the actual mode field diameter of the beam incident on the exit fiber end face. These formulae can be obtained by approximating the fundamental mode of the fiber as a Gaussian beam, as described by Marcuse in [22], [23].

Losses at the displayed pitch of 35 µm reach a maximum of 0.24 dB, with the majority (0.15 dB) resulting from the lateral displacement of the image from the intended exit fiber core. For a $\rho = 100$ µm fiber however the losses can reach 3 dB for a maximum actuator angle of 25 degrees. It is important to note however that these losses will only be suffered on the outer-most cores of the fiber: the inner cores suffer less lateral displacement and the central core will only experience losses due to mode field diameter mismatch.

Moreover, in reality losses are likely to be dominated by misalignment within the switch, due to manufacturing tolerances and actuator pointing accuracy, as well as optical aberrations within the system as a whole. Angled incidence on a real lens causes further aberrations to the image created on the exit fiber that is not observed within the thin lens approximation. Experimentally, the total loss of the previously demonstrated 4 core 1×2 switch was found to be in the range 1.23 dB to 2.21 dB [17].

Accordingly, we calculated the estimated losses caused by both angular and lateral misalignment between the input collimator and lens array, for a range of values of ρ. The value of $\rho = 25$ µm is equivalent to the 4 core MCF fibre design used in the previous experimental demonstration [17], whilst $\rho = 100$ µm represents the largest ρ considered in the paper (for example the 61 core 25 µm pitch used in Section 3). Both misalignment calculations assume that the output collimator is perfectly in position in the collimator array. Since the switch is optically symmetric, an additional offset in the position or angle of the output collimator is equivalent to the net offset being applied to input collimator. This net offset could be smaller or greater than each individual offset, depending on whether the misalignments are in complementary or different directions. Moreover, the loss is the same across all cores in any given fibre since the misalignments shift the entire image that is focussed onto the exit fibre end face.

The results are displayed in Fig. 8. That an angular misalignment of only 0.03 degrees is sufficient to cause 1 dB of loss in 25/35 µm case highlights the importance of collimator pointing accuracy in this beam steering switch design. However, an angular offset of the entire collimator array would be simple to correct in software providing that the actuators are able to achieve the required accuracy.

Perhaps counter intuitively, fibres with large values of ρ are more tolerant to angular misalignment. This can be explained by considering that to accommodate a fibre with large ρ, whether due to a high core count or large core pitch, smaller values of f_1 and f_2, and consequently z_1 and z_2, must be used. This results in a shorter distance (z_2) for the

This article has been accepted for publication in a future issue of this journal, but has not been fully edited. Content may change prior to final publication. Citation information: DOI 10.1109/JLT.2019.2896318, Journal of Lightwave Technology

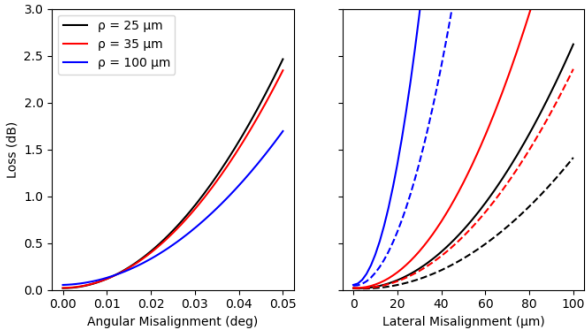

Fig. 8. Estimated total losses across all cores resulting from both angular and lateral misalignment between the collimator and lens array, for $\rho = 25\,\mu\text{m}$, $35\,\mu\text{m}$, $100\,\mu\text{m}$. Dashed lines indicate a MFD of $12\,\mu\text{m}$, solid lines indicate a MFD of $8\,\mu\text{m}$. The maximum actuator angle is 10 degrees and the loss is wavelength independent.

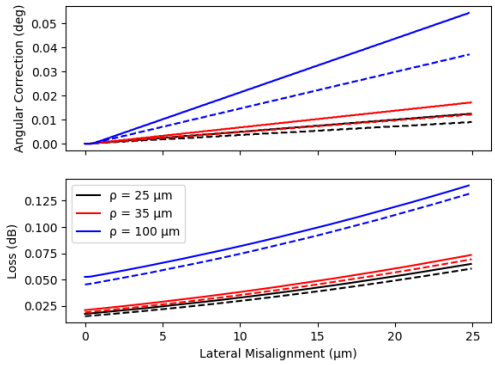

Fig. 9. Required angular correction to compensate for a given lateral misalignment at the collimator, for $\rho = 25\,\mu\text{m}$, $35\,\mu\text{m}$, $100\,\mu\text{m}$. Dashed lines indicate a MFD of $12\,\mu\text{m}$, solid lines indicate a MFD of $8\,\mu\text{m}$. The maximum actuator angle is 10 degrees and the loss is wavelength independent.

beam to propagate within the switch, meaning that angular misalignments translate to shorter lateral shift on the exit fibre end face and lower resultant losses.

On the other hand, a lateral misalignment of approximately $50\,\mu\text{m}$ (for an MFD of $8\,\mu\text{m}$) between the collimators and lens array in the $35\,\mu\text{m}$ case is enough to cause a 1 dB loss within the switch. Larger values of ρ result in significantly higher losses for the same lateral misalignment: the smaller z_1/z_2 values used in high ρ switches mean that an equivalent shift represents a larger disturbance to the system.

The dependence of loss on MFD can also be seen in Fig. 8 Larger MFDs appear more tolerant to this lateral misalignment loss, with a lateral misalignment of $70\,\mu\text{m}$ required to cause the equivalent 1 dB loss in the $35\,\mu\text{m}$ case for an MFD of $12\,\mu\text{m}$. The reasons for why angular misalignment loss does not exhibit this MFD dependence is evident once the characteristics of each misalignment mechanism is examined. It should be restated that the losses for each MFD are calculated through systems that have been optimized for the specified MFD, essentially meaning that the scale of the system (in terms of the z_1 and z_2 distances) has been 'normalized' to its respective MFD. Thus as an angular misalignment is indifferent to the physical system scale, it does not change the losses with respect to the MFD. This is not the case with the lateral misalignment, which will have a larger impact on a switch of smaller scale (or MFD).

One strategy to counter lateral misalignments in particular might be to compensate by adjusting the actuator angle to the new required beam path. In this sense, a deliberate angular 'misalignment' might be used to correct an unintended lateral misalignment. This correction could be applied in software post device manufacture, providing that the collimator pointing accuracy is sufficiently accurate. In Fig. 9, we present the angular correction required for a given lateral misalignment to minimise the loss, along with the resultant loss when this correction is applied. The loss can be reduced for example by 0.13 dB (from 0.19 dB to 0.06 dB) for a $\rho = 35\,\mu\text{m}$, $8\,\mu\text{m}$ MFD fiber and by 1.15 dB (from 1.27 dB to 0.12 dB) for a $\rho = 100\,\mu\text{m}$, $8\,\mu\text{m}$ for a lateral misalignment of $20\,\mu\text{m}$. Larger values of ρ however require a larger correction to compensate for the same misalignment. The value of this technique is limited however, since the angular correction causes beam clipping on the output lens collimator once the lateral misalignment and required correction becomes too large. For the designs presented in this paper, which ensure that the beams remain within a 5% margin of the lens apertures, this occurs at approximately $25\,\mu\text{m}$.

The final potential source of additional system losses is the variation in the core pitch. The pitch of cores in a multicore can vary substantially from the specified pitch due to inconsistencies in the manufacturing processes. Typical variations (or offsets) from the desired pitch are in the range $0.1\,\mu\text{m}$ to $1\,\mu\text{m}$, with larger pitches typically exhibiting greater uncertainty [24], [25]. Since a core offset, whether on the input or output fibre, simply shifts the core image by the same amount on the exit fibre end face, the loss is independent of wavelength, MFD or core pitch (or ρ). Fig. 10 shows the estimated total losses for a given core pitch offset, with a offset of approximately $1\,\mu\text{m}$ resulting in 0.3 dB loss. In the worst possible case, and offset of $1\,\mu\text{m}$ in both fibres in opposite directions could lead to a net offset of $2\,\mu\text{m}$ and losses of 1.1 dB. Maintaining accuracy in the MCF manufacturing process is therefore key to achieving a low loss switch as well as loss uniformity across the cores, which is a more serious challenge for more complex fibre structures.

The trends from these simulations indicate that the experimental losses experienced in [17] can likely be attributed to lateral/angular misalignments or variations in the core pitch. Finally, it is important to emphasize that these losses are not unique to the multicore switch. They are universal to any beam steering switch of the design outlined in Fig. 1, whether the fibers involved are single core or multicore, yet are significantly enhanced for high core count MCFs.

III. Fiber Design

This section considers how the fiber design affects the three main performance parameters described in Section 1. As demonstrated by Fig. 5 and 6, the maximum connectivity of the switch is affected by the core MFD, wavelength, and

This article has been accepted for publication in a future issue of this journal, but has not been fully edited. Content may change prior to final publication. Citation information: DOI 10.1109/JLT.2019.2896318, Journal of Lightwave Technology

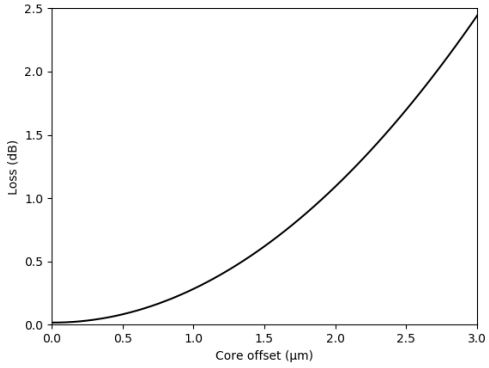

Fig. 10. Losses induced from a given offset in the core pitch. The loss is independent of wavelength, MFD, core pitch (or ρ). The actuator angle is 10 degrees.

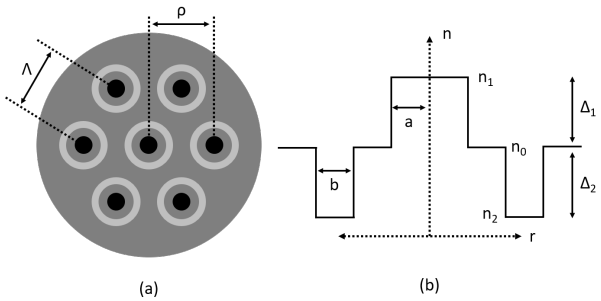

Fig. 11. (a) 7 core hexagonal TA-MCF, with core pitch, Λ, and distance from the outer most core to the fiber center, ρ. (b) Refractive index profile of a trench assisted core, n_0 is the cladding refractive index, with the core and trench index raised and lowered to n_1 and n_2 respectively.

overall width of the core structure, but these variables also change the capacity and core to core crosstalk of a fiber within a single port.

Any fiber design that seeks to maximize the capacity (or throughput) of a single port should maintain rotational symmetry in its core arrangement to achieve the maximum number of cores for a given overall width of the core structure. Suitable candidates that fit this specification include hexagonal lattice [5], two pitch structure [26], one ring structure MCFs [27] and dual ring structure [28]. In this paper we use the hexagonal MCF design as an illustrative example but all of the qualitative conclusions presented are equally applicable to any rotationally symmetric fiber design. The layout of a 7 core hexagonal MCF is shown in Fig. 11(a), with the core refractive index profile shown in Fig. 11(b). The trench assisted core structure is the focus of this work since it has been shown to minimize core to core crosstalk in multicore fiber design with the trench width, b, set equal to both the core radius, b, and the core-trench separation.

The dependence of the overall width on the maximum achievable port count is demonstrated in Fig. 12, which shows the 1 dimensional port count as a function of both ρ, the distance from the outer most core to the fiber center, and MFD. The ρ is limited to $100\,\mu\mathrm{m}$ since fibers with cladding diameters beyond $200\,\mu\mathrm{m}$ have reduced flexibility and are susceptible to

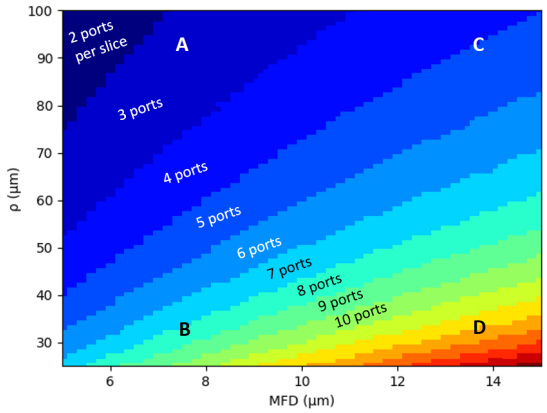

Fig. 12. One dimensional port count dependence on the two principal parameters of the fiber design: MFD and the distance from the outer most core to the fiber center, ρ. Port counts are calculated assuming that the optimal f_1/f_2 values are used for each design and a maximum actuator angle of 10 degrees.

breaking.

Reducing the overall width of the core layout and increasing the MFD both serve to increase the port count but in turn reduce the capacity of the fiber to carry more cores without significant increase in crosstalk. The annotations indicate the various regions of this graph that a switch may wish to operate, depending on the application:

A Low crosstalk, low connectivity, high capacity.
B Low crosstalk, medium connectivity, low capacity.
C High crosstalk, medium connectivity, high capacity.
D High crosstalk, high connectivity, low capacity.

Not included in this graph however is that within the overall width of the fiber the core density and core structure can be additionally tuned to fit the application. An increase in core density (to increase capacity) or MFD (to increase connectivity) will invariably cause greater core to core coupling and crosstalk. The trench assisted MCF shows its advantages here, since this core structure has been shown to reduce the coupling coefficient significantly whilst maintaining a comparable MFD.

In order to evaluate the effect of the core structure design on switch performance, we calculated the core to core mode coupling coefficients for a variety of trench assisted homogeneous fiber designs by varying both the core refractive index contrast, Δ_1, and the core radius, a. The trench depth was set to the maximum achievable by current OVD and VAD manufacturing methods ($\Delta_2 = -0.70\%$) [29], since increasing the trench depth does not significantly change the mode field diameter but does reduce the coupling coefficient. It is therefore almost always in our case advantageous to maximize the trench depth.

Mode coupling coefficients, k_{pq}, were calculated using the

analytical expression from [30]

$$k_{pq} = \frac{U_1^2}{V_1^3 K_1^2(W_1)} \sqrt{\frac{\Gamma \Delta_1 \pi}{a W_1 \Lambda}} \times \exp\left[- \frac{W_1 \Lambda + 2(W_2 - W_1)b}{a} \right] \quad (5)$$

with the following definitions

$$U_1 = a\sqrt{k_1 n_1 - \beta_1} \quad (6)$$

$$W_1 = a^2(\beta^2 - k_1^2 n_0^2) \quad (7)$$

$$W_2 = \sqrt{W_1^2 + V_2^2} \quad (8)$$

$$V_2 = ka\sqrt{n_0^2 - n_2^2} \quad (9)$$

$$\Gamma = \frac{W_1}{W_1(W_2 - W_1)b/\Lambda} \quad (10)$$

where V_1 is the normalized frequency (or V number), Λ is the core pitch, a is the core radius, b is the trench width, n_1/n_0 are the respective core/cladding refractive indices, k_1 the wave number, and K_i is the modified Bessel function of the second kind of order i. The propagation constant β_1 is specific to the exact core design and was calculated using standard methods for solving for LP modes under the weakly guiding approximation, for example as described by Okamoto in [31].

One additional penalty of increasing the MFD is that the fibre becomes more susceptible to bend loss. To account for this, macro bend loss was calculated with the following expression, first derived by Sakai and Kimura [32]

$$\alpha_{macro} = \frac{10}{\log 10} \frac{\sqrt{\pi} P_{clad}}{4a[K_{-1}(W_1)K_1(W_1) - K_0^2(W_1)]} \times \frac{1}{W_1 \sqrt{\frac{W_1 R}{a} + \frac{V^2}{2\Delta W_1}}} \exp\left[\frac{-4\Delta_1 W_1^3 R}{3aV^2} \right] \quad (11)$$

Which is expressed in dB/m. R is the bend radius and P_{clad} is the fraction of power in the cladding, determined by solving for the electric field distribution within the specific core design.

Fig. 13 shows MFD, coupling coefficient and port counts as a function of core radius and core/cladding refractive index contrast for a trench assisted 7 core hexagonal homogeneous MCF for (a) $35\,\mu\mathrm{m}$, (b) $40\,\mu\mathrm{m}$, (c) $45\,\mu\mathrm{m}$ operating at 1550 nm. The port counts are purely a function of the MFD and can be seen to follow the same contours. The red lines indicate the LP_{11} mode cutoff and show the parameters at which the core becomes multimode. A large enough refractive index contrast or core radius reduces the strength of the waveguide and eventually leads to multimode operation. The pink lines indicate a bend loss of 0.5 dB after 100 turns at a bend radius of $30\,\mathrm{mm}$.

A decrease in the core pitch causes both an increase in the port count for a given MFD and a increase in the mode coupling coefficient and therefore crosstalk. The MFD and multimode cutoff points are not affected by the core pitch since these parameters are purely dependent on the core itself.

In Fig. 14, the same parameters maps are produced but for a fixed core pitch of 35 um and for an operating wavelength of (a) 1260 nm, (b) 1550 nm, (c) 1620 nm. 1550 nm represents the minimum loss C-band whilst 1260 nm and 1620 nm represent the bottom of the O-band and top of the L-band respectively. A shorter wavelength results in both a reduced coupling coefficient and mode field diameter for a given core radius and core/cladding refractive index contrast for a given wavelength. Moreover, a reduction in the wavelength also leads to an increase in the port count for a given core design as previously shown in Fig. 5 and Fig. 6. However, shorter wavelengths also result in a decreased parameter space for single mode operation.

The coupling coefficient maps in Fig. 13 and 14 were calculated for a range of wavelengths from 1260 nm to 1620 nm and pitches from $25\,\mu\mathrm{m}$ to $100\,\mu\mathrm{m}$ with core radii ranging from $1\,\mu\mathrm{m}$ to $8\,\mu\mathrm{m}$ and core/cladding refractive index contrast ranging from 0.1% to 0.8%. By determining the coupling coefficients at the intercepts of the single/multi mode interface and port contours, we could find the fibre core design, in terms of core/cladding refractive index contrast and core radius, that would give the minimum crosstalk for a specific port count, wavelength and pitch. We assume a maximum actuator angle of 10 degrees and enforce the condition that the bend loss does not exceed 0.5 dB after 100 turns at a bend radius of $30\,\mathrm{mm}$, i.e. that the point lies above the pink lines in Fig. 13 and 14.

Once the minimum core to core coupling coefficient was obtained this allowed for a estimation of the core to core crosstalk. The statistical mean crosstalk per meter for a homogeneous MCF [33], or power leakage from one core to another, is given by

$$\mu = \frac{2\kappa^2 R}{\beta \Lambda} \quad (12)$$

Where κ is the core to core coupling coefficient and R is the bend radius, which is assumed to be 500 mm. From the core to core crosstalk, we can then calculate the overall crosstalk on a particular core, assuming unidirectional transmission, with

$$\mathrm{XT} = \frac{n - ne^{-(n+1)2\mu L}}{1 + ne^{-(n+1)2\mu L}} \quad (13)$$

Where n is the number of neighboring cores. The numerator and denominator represent the total signal power of the target core and surrounding cores respectively, calculated over a length, L.

Note that in this paper we only consider the transmission crosstalk between cores in the MCF. Crosstalk from the switch itself is negligible in comparison: an analysis of power leakage using a similar approach used to calculate the losses in the previous section reveals that any crosstalk caused by misalignment in the switch, due to lateral shifts in beam position or MFD mismatch, is always several orders of magnitude lower than that generated as the signal is transmitted through the fiber spans, even after a transmission distance of only 10 m. For example, the estimated power leakage for a 12um MFD mode is -75 dB at a distance of 25um. Crucially, as these misalignments also cause an exponential increase in losses so

This article has been accepted for publication in a future issue of this journal, but has not been fully edited. Content may change prior to final publication. Citation information: DOI 10.1109/JLT.2019.2896318, Journal of Lightwave Technology

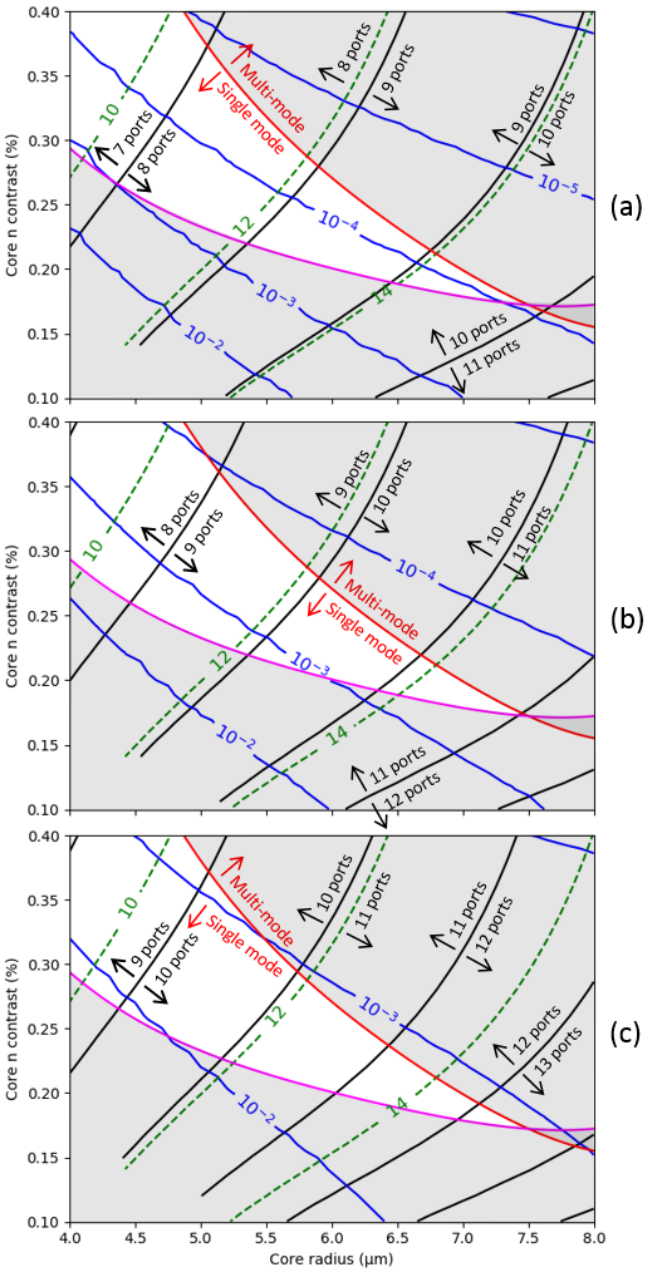

Fig. 13. Core design parameter maps for a trench assisted 7 core hexagonal homogeneous MCF for (a) 45 μm, (b) 40 μm, (c) 35 μm pitch operating at 1550 nm. Blue and green contours show the resultant mode coupling coefficients (m^{-1}) and MFDs (μm) respectively. The allowable parameters are bound by the LP_{11} mode cutoff (red) and the maximum loss of 0.5 dB per 100 turns at 30 mm bend radius (pink): parameters outside of these bounds are designated by shading. Port counts are calculated using the optimal f_1/f_2 values and assuming a maximum actuator angle of 10 degrees.

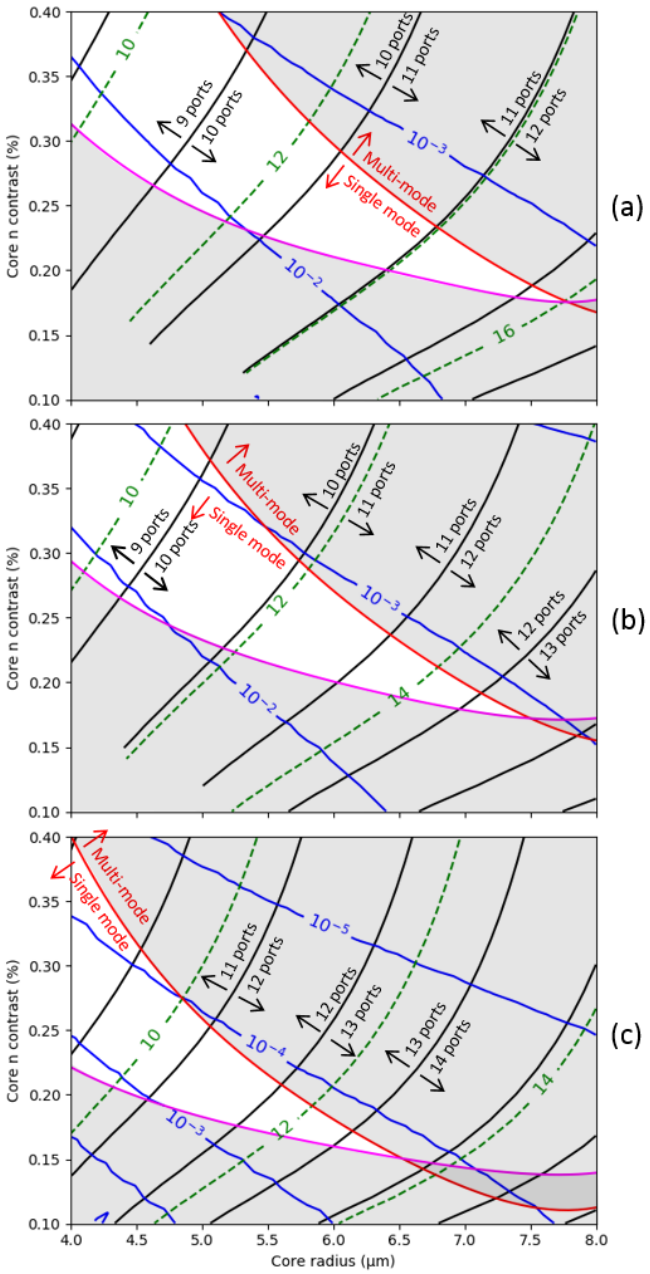

Fig. 14. Core design parameter maps for a 35 um pitch trench assisted 7 core hexagonal homogeneous MCF operating at (a) 1620 nm, (b) 1550 nm, (c) 1260 nm. Blue and green contours show the resultant mode coupling coefficients (m^{-1}) and MFDs (μm) respectively. The allowable parameters are bound by the LP_{11} mode cutoff (red) and the maximum loss of 0.5 dB per 100 turns at 30 mm bend radius (pink): parameters outside of these bounds are designated by shading. Port counts are calculated using the optimal f_1/f_2 values and assuming a maximum actuator angle of 10 degrees.

as to render the switch inoperable before any significant level of switch crosstalk occurs.

Fig. 15 shows the total crosstalk after 1 km on the central core of 7, 19 and 37 core hexagonal TA-MCF for the minimum achievable core to core coupling coefficient at 1550 nm, assuming a maximum collimator angle of 10 degrees. In every case, an increase in core pitch (or decrease in core density) leads to a logarithmic decrease in the total crosstalk on the central core due to the decreased core to core coupling. The maximum pitch for each configuration is defined by the aforementioned maximum cladding diameter of 100 μm.

Increasing either the core count (capacity) or port count (connectivity) imposes a crosstalk talk penalty on the system. Higher port counts require a larger MFD to reduce beam

This article has been accepted for publication in a future issue of this journal, but has not been fully edited. Content may change prior to final publication. Citation information: DOI 10.1109/JLT.2019.2896318, Journal of Lightwave Technology

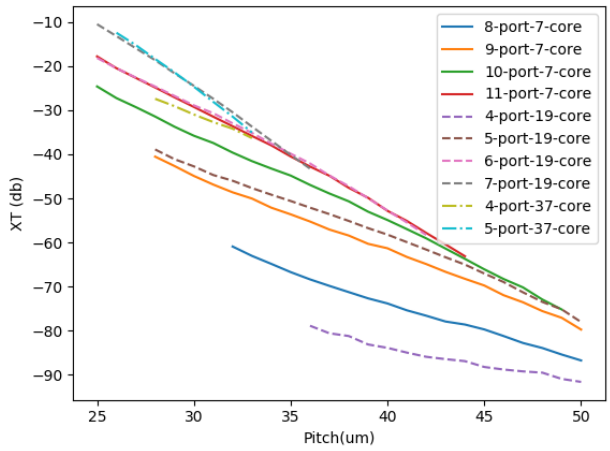

Fig. 15. Total crosstalk (XT) after 1 km on the central core of a 7/19/37 core hexagonal homogeneous TA-MCF for the minimum value of mode coupling coefficient at which single mode operation is maintained, operating at 1550 nm. Port counts are calculated assuming that the optimal f_1/f_2 values are used for each design.

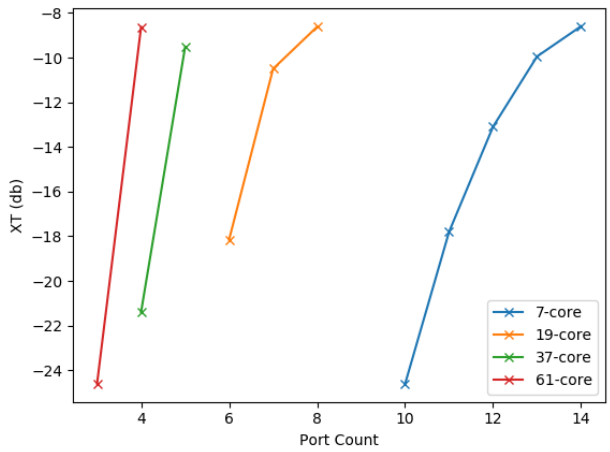

Fig. 16. Total crosstalk (XT) after 1 km on the central core of a 7/19/37/61 core hexagonal homogeneous TA-MCF for the minimum value of mode coupling coefficient at which single mode operation is maintained, with a fixed pitch of 25 µm, operating at a wavelength of 1550 nm. Port counts are calculated assuming that the optimal f_1/f_2 values are used for each design.

spreading and prevent beam clipping at the lenses, which leads to higher crosstalk if it is to remain single mode and maintain a reasonable level of bend loss. Higher core counts also impose a significant crosstalk penalty, since cores must be packed more tightly to obtain the same port count as a lower core count design, in addition to increased net crosstalk from the extra outer cores.

These penalties are demonstrated more clearly in Fig. 16, which shows the total crosstalk on the central core of a homogeneous hexagonal TA-MCF as a function of port count for a fixed pitch of 25 µm operating at 1550 nm. For example, increasing the port count on a 7 core fiber from 10 to 11 leads to a 6 dB penalty on the central core, whilst increasing the port count from 3 to 4 on a 61 core suffers a 16 dB crosstalk increase.

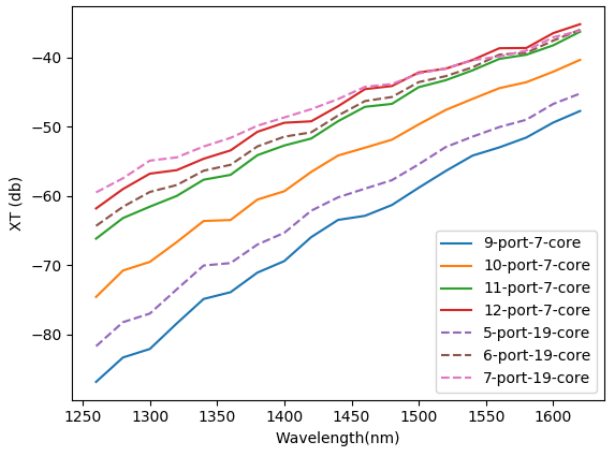

Fig. 17. Total crosstalk (XT) after 1 km on the central core of a 7/19 core hexagonal homogeneous TA-MCF for the minimum value of mode coupling coefficient at which single mode operation is maintained, with a fixed pitch of 25 µm. Port counts are calculated assuming that the optimal f_1/f_2 values are used for each design.

Translating these port counts to 2D reveals that a potential high capacity, low connectivity system from Fig. 16 is a 5 port switch utilizing a 61 core TA-MCF with -25 dB crosstalk after 1 km. Conversely, a high connectivity, low capacity 100 port switch with similar crosstalk is demonstrated with a 7 core hexagonal TA-MCF. Low crosstalk configurations are also possible, for example -80 dB for a 8 port switch using a 19 core TA-MCF in Fig. 16. The crosstalk thresholds are heavily influenced by the modulation format: simple on-off keying that is typically deployed in DCNs can tolerate a larger amount of crosstalk than the higher order formats that are often used in metro and core networks [34].

Fig. 17 shows the wavelength dependent crosstalk for a fixed pitch. Shorter wavelengths are beneficial for crosstalk reduction since they reduce the mode coupling coefficients for a given core design, as shown in Fig. 14, as well as reduction in the MFD which reduces beam spreading in the system. Shorter wavelengths therefore can offer better connectivity or capacity for a fixed crosstalk, although care must be taken to consider the increased losses incurred when deviating from the minimum silica loss wavelength of 1550 nm.

Fig. 18 shows the dependence of crosstalk on the link distance for a selection of switch and core configurations, for a pitch of 35 µm and operating at a wavelength of 1550 nm. The link distances displayed range from 1 km (DCNs) to 100 km (metro network) to 1000 km (core network). Choosing a sufficiently low core and port count (sacrificing capacity and connectivity) allows for a configurations that can be utilized for metro and core link applications. For example, -25 db crosstalk after 100 km is achievable for a 50 port switch using a 7 core TA-MCF. Similar levels of crosstalk can be accomplished at 1000 km for a 41 port switch using a 7 core TA-MCF.

This article has been accepted for publication in a future issue of this journal, but has not been fully edited. Content may change prior to final publication. Citation information: DOI 10.1109/JLT.2019.2896318, Journal of Lightwave Technology

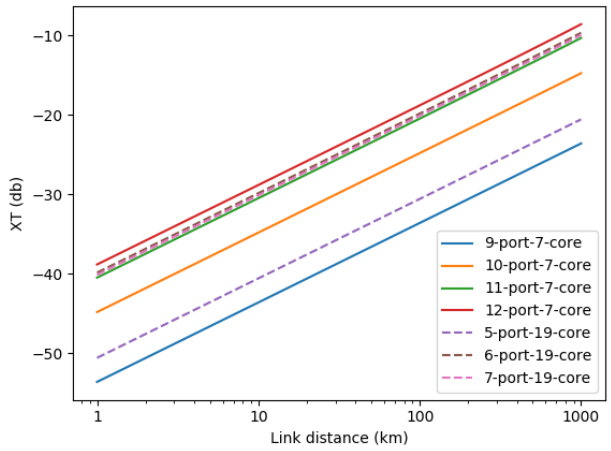

Fig. 18. Total crosstalk (XT) on the central core of a 7/19 core hexagonal homogeneous TA-MCF for the minimum value of mode coupling coefficient at which single mode operation is maintained, with a fixed pitch of 35 µm, operating at a wavelength of 1550 nm. Port counts are calculated assuming that the optimal f_1/f_2 values are used for each design.

A bi-directional core assignment scheme can further reduce crosstalk by around 3 dB, assuming that cores transmitting in opposite directions experience a power leakage reduction of 20 dB [35], but this is not presented here as it is independent of the switch design. Unfortunately, comparison of the crosstalk values calculated here to the previous practical demonstration in [17] are limited since the experimental values obtained were attributed to fan in/out devices, not the switch itself.

IV. Conclusion

This paper has detailed the design and performance characteristics of a free space beam steering switch for multi core fibers that have become of increasing interest for space division multiplexing applications. Either port count, core count and crosstalk can be maximized at the expense of the others depending on the whether the required application emphasizes connectivity, fiber capacity or minimizing crosstalk. Potential losses from system misalignments and fiber fabrication variations in the core pitch are also estimated, and may offer significant practical challenges when integrating high core count MCFs into the switch design.

Our studies show that a 50 port switch is possible for a 25 µm core pitch 7 core hexagonal TA-MCF with a total mean statistical crosstalk on the central core of -25 dB after 1 km, assuming an operational wavelength of 1550 nm and maximum collimator actuator angle of 10 degrees. In contrast, a high capacity 25 µm core pitch 61 core hexagonal TA-MCF can still offer up to a 5 port switch for the same level of crosstalk. Low crosstalk configurations are also possible, for example -80 dB for a 8 port switch using a 19 core hexagonal TA-MCF. For metro and core networks, a -25 db crosstalk after 100 km is achievable for a 50 port switch using a 35 µm core pitch 7 core TA-MCF, whilst similar levels of crosstalk can be accomplished at 1000 km for a 41 port switch using a 35 µm core pitch 7 core TA-MCF.

Higher performance is offered at shorter wavelengths and higher actuator angles, although both can lead to increased system losses. Further studies would involve more extensive experimental work to expand on [17] and verify the calculations presented here, including the manufacturing of the suggested fiber designs.

References

[1] R. Essiambre and R. W. Tkach, "Capacity Trends and Limits of Optical Communication Networks," *Proceedings of the IEEE*, vol. 100, pp. 1035–1055, May 2012.

[2] D. J. Richardson, J. M. Fini, and L. E. Nelson, "Space-division multiplexing in optical fibres," *Nature Photonics*, vol. 7, pp. 354–362, May 2013.

[3] J. Sakaguchi, B. J. Puttnam, W. Klaus, Y. Awaji, N. Wada, A. Kanno, T. Kawanishi, K. Imamura, H. Inaba, K. Mukasa, R. Sugizaki, T. Kobayashi, and M. Watanabe, "305 Tb/s Space Division Multiplexed Transmission Using Homogeneous 19-Core Fiber," *Journal of Lightwave Technology*, vol. 31, pp. 554–562, Feb. 2013.

[4] T. Hayashi, T. Taru, O. Shimakawa, T. Sasaki, and E. Sasaoka, "Low-crosstalk and low-loss multi-core fiber utilizing fiber bend," in *2011 Optical Fiber Communication Conference and Exposition and the National Fiber Optic Engineers Conference*, pp. 1–3, Mar. 2011.

[5] K. Takenaga, Y. Arakawa, S. Tanigawa, N. Guan, S. Matsuo, K. Saitoh, and M. Koshiba, "Reduction of crosstalk by trench-assisted multi-core fiber," in *2011 Optical Fiber Communication Conference and Exposition and the National Fiber Optic Engineers Conference*, pp. 1–3, Mar. 2011.

[6] M. Koshiba, K. Saitoh, and Y. Kokubun, "Heterogeneous multi-core fibers: proposal and design principle," *IEICE Electronics Express*, vol. 6, no. 2, pp. 98–103, 2009.

[7] K. Saitoh, M. Koshiba, K. Takenaga, and S. Matsuo, "Crosstalk and Core Density in Uncoupled Multicore Fibers," *IEEE Photonics Technology Letters*, vol. 24, pp. 1898–1901, Nov. 2012.

[8] T. Hayashi, A. Mekis, T. Nakanishi, M. Peterson, S. Sahni, P. Sun, S. Freyling, G. Armijo, C. Sohn, D. Foltz, T. Pinguet, M. Mack, Y. Kaneuchi, O. Shimakawa, T. Morishima, T. Sasaki, and P. De Dobbelaere, "End-to-End Multi-Core Fibre Transmission Link Enabled by Silicon Photonics Transceiver with Grating Coupler Array," Sept. 2017.

[9] W. Klaus, B. J. Puttnam, R. S. Luis, J. Sakaguchi, J. D. Mendinueta, Y. Awaji, and N. Wada, "Advanced space division multiplexing technologies for optical networks [Invited]," *IEEE/OSA Journal of Optical Communications and Networking*, vol. 9, pp. C1–C11, Apr. 2017.

[10] M. D. Feuer, L. E. Nelson, X. Zhou, S. L. Woodward, R. Isaac, B. Zhu, T. F. Taunay, M. Fishteyn, J. M. Fini, and M. F. Yan, "Joint Digital Signal Processing Receivers for Spatial Superchannels," *IEEE Photonics Technology Letters*, vol. 24, pp. 1957–1960, Nov. 2012.

[11] P. J. Winzer, D. T. Neilson, and A. R. Chraplyvy, "Fiber-optic transmission and networking: the previous 20 and the next 20 years [Invited]," *Optics Express*, vol. 26, pp. 24190–24239, Sept. 2018.

[12] R. Ryf, S. Chandrasekhar, S. Randel, D. T. Neilson, N. K. Fontaine, and M. Feuer, "Physical layer transmission and switching solutions in support of spectrally and spatially flexible optical networks," *IEEE Communications Magazine*, vol. 53, pp. 52–59, Feb. 2015.

[13] S. Yan, E. Hugues-Salas, V. J. F. Rancao, Y. Shu, G. M. Saridis, B. R. Rofoee, Y. Yan, A. Peters, S. Jain, T. May-Smith, P. Petropoulos, D. J. Richardson, G. Zervas, and D. Simeonidou, "Archon: A Function Programmable Optical Interconnect Architecture for Transparent Intra and Inter Data Center SDM/TDM/WDM Networking," *Journal of Lightwave Technology*, vol. 33, pp. 1586–1595, Apr. 2015.

[14] L. E. Nelson, M. D. Feuer, K. Abedin, X. Zhou, T. F. Taunay, J. M. Fini, B. Zhu, R. Isaac, R. Harel, G. Cohen, and D. M. Marom, "Spatial Superchannel Routing in a Two-Span ROADM System for Space Division Multiplexing," *Journal of Lightwave Technology*, vol. 32, pp. 783–789, Feb. 2014.

[15] G. M. Saridis, D. Alexandropoulos, G. Zervas, and D. Simeonidou, "Survey and Evaluation of Space Division Multiplexing: From Technologies to Optical Networks," *IEEE Communications Surveys Tutorials*, vol. 17, no. 4, pp. 2136–2156, 2015.

[16] G. Zervas, H. Yuan, A. Saljoghei, Q. Chen, and V. Mishra, "Optically disaggregated data centers with minimal remote memory latency: Technologies, architectures, and resource allocation [Invited]," *IEEE/OSA Journal of Optical Communications and Networking*, vol. 10, pp. A270–A285, Feb. 2018.

[17] H. C. H. Mulvad, A. Parker, B. King, D. Smith, M. Kovacs, S. Jain, J. Hayes, M. Petrovich, D. J. Richardson, and N. Parsons, "Beam-steering all-optical switch for multi-core fibers," in *2017 Optical Fiber Communications Conference and Exhibition (OFC)*, pp. 1–3, Mar. 2017.

[18] N. Parsons, A. Hughes, and R. Jensen, "High Radix All-Optical Switches for Software-Defined Datacentre Networks," in *ECOC 2016; 42nd European Conference on Optical Communication*, pp. 1–3, Sept. 2016.

[19] J. Arnaud, "Representation of Gaussian beams by complex rays," *Applied Optics*, vol. 24, pp. 538–543, Feb. 1985.

[20] J. E. Harvey, R. G. Irvin, and R. N. Pfisterer, "Modeling physical optics phenomena by complex ray tracing," *Optical Engineering*, vol. 54, p. 035105, Mar. 2015.

[21] R. Herloski, S. Marshall, and R. Antos, "Gaussian beam ray-equivalent modeling and optical design," *Applied Optics*, vol. 22, pp. 1168–1174, Apr. 1983.

[22] D. Marcuse, "Excitation of the dominant mode of a round fiber by a Gaussian beam," *The Bell System Technical Journal*, vol. 49, pp. 1695–1603, Oct. 1970.

[23] D. Marcuse, "Loss analysis of single-mode fiber splices," *The Bell System Technical Journal*, vol. 56, pp. 703–718, May 1977.

[24] T. Hayashi, T. Nagashima, K. Yonezawa, Y. Wakayama, D. Soma, K. Igarashi, T. Tsuritani, T. Taru, and T. Sasaki, "Six-Mode 19-Core Fiber With 114 Spatial Modes for Weakly-Coupled Mode-Division-Multiplexed Transmission," *Journal of Lightwave Technology*, vol. 35, pp. 748–754, Feb. 2017.

[25] T. Matsui, T. Kobayashi, H. Kawahara, E. L. T. d. Gabory, T. Nagashima, T. Nakanishi, S. Saitoh, Y. Amma, K. Maeda, S. Arai, R. Nagase, Y. Albe, S. Aozasa, Y. Wakayama, H. Takeshita, T. Tsuritani, H. Ono, T. Sakamoto, I. Morita, Y. Miyamoto, and K. Nakajima, "118.5 Tbit/s transmission over 316 km-long multi-core fiber with standard cladding diameter," in *2017 Opto-Electronics and Communications Conference (OECC) and Photonics Global Conference (PGC)*, pp. 1–2, July 2017.

[26] S. Matsuo, K. Takenaga, Y. Arakawa, Y. Sasaki, S. Taniagwa, K. Saitoh, and M. Koshiba, "Large-effective-area ten-core fiber with cladding diameter of about 200 m," *Optics Letters*, vol. 36, p. 4626, Dec. 2011.

[27] H. Takara, A. Sano, T. Kobayashi, H. Kubota, H. Kawakami, A. Matsuura, Y. Miyamoto, Y. Abe, H. Ono, K. Shikama, Y. Goto, K. Tsujikawa, Y. Sasaki, I. Ishida, K. Takenaga, S. Matsuo, K. Saitoh, M. Koshiba, and T. Morioka, "1.01-Pb/s (12 SDM/222 WDM/456 Gb/s) Crosstalk-managed Transmission with 91.4-b/s/Hz Aggregate Spectral Efficiency," in *European Conference and Exhibition on Optical Communication*, (Amsterdam, The Netherlands), p. Th.3.C.1, OSA, 2012.

[28] A. Sano, H. Takara, T. Kobayashi, H. Kawakami, H. Kishikawa, T. Nakagawa, Y. Miyamoto, Y. Abe, H. Ono, K. Shikama, M. Nagatani, T. Mori, Y. Sasaki, I. Ishida, K. Takenaga, S. Matsuo, K. Saitoh, M. Koshiba, M. Yamada, H. Masuda, and T. Morioka, "409-Tb/s + 409-Tb/s crosstalk suppressed bidirectional MCF transmission over 450 km using propagation-direction interleaving," *Optics Express*, vol. 21, p. 16777, July 2013.

[29] F. Ye, J. Tu, K. Saitoh, K. Takenaga, S. Matsuo, H. Takara, and T. Morioka, "Design of Homogeneous Trench-Assisted Multi-Core Fibers Based on Analytical Model," *Journal of Lightwave Technology*, vol. 34, pp. 4406–4416, Sept. 2016.

[30] F. Ye, J. Tu, K. Saitoh, and T. Morioka, "Simple analytical expression for crosstalk estimation in homogeneous trench-assisted multi-core fibers," *Optics Express*, vol. 22, p. 23007, Sept. 2014.

[31] K. Okamoto, *Fundamentals of optical waveguides*. Amsterdam ; Boston: Elsevier, 2nd ed ed., 2006.

[32] J.-i. Sakai and T. Kimura, "Bending loss of propagation modes in arbitrary-index profile optical fibers," *Applied Optics*, vol. 17, p. 1499, May 1978.

[33] T. Hayashi, T. Taru, O. Shimakawa, T. Sasaki, and E. Sasaoka, "Design and fabrication of ultra-low crosstalk and low-loss multi-core fiber," *Optics Express*, vol. 19, p. 16576, Aug. 2011.

[34] P. J. Winzer, A. H. Gnauck, A. Konczykowska, F. Jorge, and J. Dupuy, "Penalties from in-band crosstalk for advanced optical modulation formats," in *2011 37th European Conference and Exhibition on Optical Communication*, pp. 1–3, Sept. 2011.

[35] H. Yuan, M. Furdek, A. Muhammad, A. Saljoghei, L. Wosinska, and G. Zervas, "Space-division multiplexing in data center networks: on multi-core fiber solutions and crosstalk-suppressed resource allocation," *IEEE/OSA Journal of Optical Communications and Networking*, vol. 10, pp. 272–288, Apr. 2018.